Atmos. Chem. Phys. Discuss., 14, 31039–31090, 2014
www.atmos-chem-phys-discuss.net/14/31039/2014/
doi:10.5194/acpd-14-31039-2014

Atmospheric Chemistry and Physics Discussions

Evaluation of a regional chemistry transport model using a newly developed regional OMI NO_2 retrieval

G. Kuhlmann[1,*], Y. F. Lam[1], H. M. Cheung[1], A. Hartl[1], J. C. H. Fung[2], P. W. Chan[3], and M. O. Wenig[4]

[1]School of Energy and Environment, City University of Hong Kong, Hong Kong, China
[2]Department of Mathematics, The Hong Kong University of Science & Technology, Hong Kong, China
[3]Hong Kong Observatory, Hong Kong, China
[4]Meteorologisches Institut, Ludwig-Maximilians-Universität, Munich, Germany
[*]now at: Empa, Swiss Federal Laboratories for Materials Science and Technology, Dübendorf, Switzerland

Received: 26 September 2014 – Accepted: 7 November 2014 – Published: 9 December 2014

Correspondence to: G. Kuhlmann (gerrit.kuhlmann@gmail.com) and
Y. F. Lam (yunflam@cityu.edu.hk)

Published by Copernicus Publications on behalf of the European Geosciences Union.

Abstract

In this paper, we evaluate a high-resolution chemistry transport model (CTM) (3 km × 3 km spatial resolution) with the new Hong Kong (HK) NO_2 retrieval developed for the Ozone Monitoring Instrument (OMI) on-board the Aura satellite. The three-dimensional atmospheric chemistry was modelled in the Pearl River Delta (PRD) region in southern China by the Models-3 Community Multiscale Air Quality (CMAQ) modelling system from October 2006 to January 2007. In the HK NO_2 retrieval, tropospheric air mass factors (AMF) were recalculated using high-resolution ancillary parameters of surface reflectance, NO_2 profile shapes and aerosol profiles of which the latter two were taken from the CMAQ simulation. We also tested four different aerosol parametrizations. Ground level measurements by the PRD Regional Air Quality Monitoring (RAQM) network were used as additional independent measurements.

The HK NO_2 retrieval increases the NO_2 vertical column densities (VCD) by (+31 ± 38) %, when compared to NASA's standard product (SP2), and reduces the mean bias (MB) between satellite and ground measurements by 26 percentage points from −41 to −15 %. The correlation coefficient r is low for both satellite datasets ($r = 0.35$) due to the high spatial variability of NO_2 concentrations.

The correlation between CMAQ and the RAQM network is low ($r \approx 0.3$) and the model underestimates the NO_2 concentrations in the north-western model domain (Foshan and Guangzhou). We compared the CMAQ NO_2 time series of the two main plumes with our regional OMI NO_2 product. The model overestimates the NO_2 VCDs by about 15 % in Hong Kong and Shenzhen, while the correlation coefficient is satisfactory ($r = 0.56$). In Foshan and Guangzhou, the correlation is low ($r = 0.37$) and the model underestimates the VCDs strongly (MB = −40 %). In addition, we estimated that the OMI VCDs are also underestimated by about 10 to 20 % in Foshan and Guangzhou because of the influence of the model parameters on the AMF.

In this study, we demonstrate that the HK OMI NO_2 retrieval reduces the bias of the satellite measurements and thus the dataset can be used to study the magnitude of

ACPD
14, 31039–31090, 2014

NO_2 concentrations in a regional model. The low bias can be achieved if AMFs are recalculated with more accurate surface reflectance, aerosol profiles and NO_2 profiles; only NO_2 profiles have been replaced in earlier studies. Since unbiased concentrations are important, for example, in air pollution studies, the results of this paper can be very helpful in future model evaluation studies.

1 Introduction

Nitrogen oxides ($NO_x = NO + NO_2$) play an important role in atmospheric chemistry. They have a vital role in the formation of photochemical smog (Haagen-Smit, 1952) and can damage crops and buildings as a component of acid rain (Driscoll et al., 2001). In an urban environment, NO_2 concentrations have a high spatial and temporal variability due to its short tropospheric life time and the variety of sources and sinks. The spatial and temporal distribution can be studied with chemistry transport models (CTM) and satellite instruments.

The first satellite instrument able to detect tropospheric NO_2 was the Global Ozone Monitoring Experiment (GOME) which was launched on board the second European Remote Sensing satellite (ERS-2) in 1995 (Burrows et al., 1999). Successor instruments to GOME (GOME-2) are payload on the MetOp satellites used for operational meteorology (Callies et al., 2000). In 2006, the Scanning Imaging Absorption Spectrometer for Atmospheric Cartography (SCIMACHY) was launched on board ENVISAT (ENVIronmental SATellite) (Bovensmann et al., 1999) and in 2004, the Ozone Monitoring Instrument (OMI) was launched on board the EOS (Earth Observation System) Aura (Levelt et al., 2006). Since the launch of GOME, the spatial resolution of the instruments increased rapidly. While GOME had a smallest ground pixel size of 40 km × 320 km, OMI has a ground pixel size of 13 km × 24 km. The higher spatial resolution makes OMI feasible for the study of trace gases in large metropolitan areas.

The two OMI NO_2 standard products are the NASA standard product (SP) (Bucsela et al., 2006, 2013) and the the Dutch OMI NO_2 product (DOMINO) (Boersma et al.,

ACPD
14, 31039–31090, 2014

2007, 2011) which are both available in their second version (SP2 and DOMINO-2). In this paper, we use the term "global" products for this two products because they provide global coverage. In contrast, "regional" products provide regional coverage. Examples of regional OMI NO_2 products are the Empa product for Europe (Boersma et al., 2007; Zhou et al., 2009, 2010) and the Berkeley High-Resolution (BEHR) product for North America (Russell et al., 2011). It should be noted that in literature the term "global" is often used as a synonym for "level 3" data that has had orbit-level data ("level 2") combined onto a global grid. This terminology can be misleading, because "level 3" data can also be provided on a local or regional grid. For example, the grid can be the domain of a regional CTM. A second difference between regional and global products is the spatiotemporal resolution of the ancillary parameters used in their retrieval algorithms. Ancillary parameters are information about surface reflectance, NO_2 profile shapes, aerosols and clouds which are used to calculate air mass factors (AMF) which convert the retrieved slant column densities (SCD) to vertical column densities (VCD). In the first version of SP and DOMINO, the ancillary parameters were mainly monthly or annual averages with spatial resolutions between 50 and 300 km. In contrast, regional products use ancillary parameters with a higher spatial and temporal resolution. For example, Zhou et al. (2010) used surface reflectance with 1 km spatial resolution to improve the NO_2 retrieval in Europe and Russell et al. (2011) replaced the profile shapes from a global CTM with profiles from a regional CTM with a spatial resolution of 4 km. Thus, we use the terms "regional" and "global" for products which use ancillary parameters which have a spatial and temporal resolution typical for a regional or global CTM, respectively.

Russell et al. (2011) compared the BEHR product with the first version of the DOMINO and the NASA product and showed that the retrieved NO_2 VCDs are strongly impacted by terrain pressure (±20 %), surface reflectance (±40 %) and the NO_2 profile shape (−75 ± 10 %). Lin et al. (2014) showed that different ancillary parameters can have a strong impact on the NO_2 VCDs. Furthermore, the global NO_2 products have been compared with regional CTMs. Since the OMI NO_2 VCDs depend on the NO_2

ACPD
14, 31039–31090, 2014

profile shapes, the global profile shapes can and should be replaced with the profiles of the regional model (Eskes and Boersma, 2003; Boersma et al., 2005). The global OMI NO_2 products provide data for this update. Several studies evaluated regional CTMs with the global NO_2 products using updated NO_2 profiles. Herron-Thorpe et al. (2010) validated the regional air quality model AIRPACT-3 (12 km × 12 km spatial resolution) over the Pacific Northwest with the first versions of DOMINO and the NASA product. Their simulations correlate well with the monthly averaged satellite measurements for cloud free data ($r = 0.75$) as long as no wildfires are present in the model domain. Han et al. (2011) compared CMAQ simulation (30 km × 30 km) with the first DOMINO version over the Korean peninsula and found that simulated VCDs are about 50 % larger than satellite measurements. Zyrichidou et al. (2013) evaluated the Comprehensive Air Quality Model (CAMx) (10 km × 10 km) over Southeastern Europe with the second DOMINO version. They found good agreement between model and OMI VCDs ($r = 0.6$), but the model overestimated VCDs over urban areas.

In SP2 and DOMINO-2, the spatial and temporal resolutions of several ancillary parameters have been increased. For example, the products are using the OMI reflectance climatology (0.5° spatial resolution) and NO_2 profile shapes are corrected using a high-resolution topography (3 km). Nevertheless, the global products still depend on a global CTM which have limited spatial resolution. As a consequence, the global products can be biased, if NO_2 VCDs are studied on regional scale.

In this study, we evaluate a regional CTM (3 km × 3 km spatial resolution) with a regional OMI NO_2 retrieval. For this purpose, we simulated three-dimensional atmospheric chemistry with the Models-3 Community Multiscale Air Quality (CMAQ) modelling system (Byun and Schere, 2006) in the Pearl River Delta (PRD) region in southern China from October 2006 to January 2007. Furthermore, we developed a new regional NO_2 retrieval for the PRD region. In the Hong Kong (HK) NO_2 retrieval, we recalculated tropospheric AMFs using high-resolution ancillary parameters which were taken mainly from the CMAQ simulation. Thus, the retrieval does not depend on other models. Cloud height and fraction were taken from the OMI cloud product (Acar-

ACPD
14, 31039–31090, 2014

reta et al., 2004) and surface reflectance was calculated from the MODIS (Moderate-resolution Imaging Spectroradiometer) black-sky albedo (BSA) product (Wanner et al., 1997; Lucht et al., 2000). We tested different aerosol parametrizations for our new product. Aerosol extinction and absorption coefficients were computed from the model output. As additional and independent observations, ground level measurements were used from 16 stations of the PRD Regional Air Quality Monitoring (RAQM) network. To the best of our knowledge, this is the first study in which a regional OMI NO_2 product is compared with a regional CTM.

This paper is organised as follows: OMI and the retrieval of tropospheric NO_2 including the AMF calculations using the SCIATRAN radiative transfer model are described briefly in Sect. 2. The RAQM network, the CMAQ model run, the HK NO_2 retrieval are described in Sect. 3. The results are presented and discussed in Sect. 4. Finally, Sect. 5 contains further discussions and concludes this paper.

2 Background

2.1 Ozone Monitoring Instrument (OMI)

OMI is a nadir-viewing imaging spectrometer measuring Earth's reflectance spectra in the near-ultraviolet and visible wavelength range with two CCD (charge-coupled device) arrays. It was launched aboard NASA's EOS Aura satellite on 15 July 2004 (Levelt et al., 2006). The instrument provides daily global coverage at an overpass time of 13:45 ± 15 min LT. Earth reflectance spectra are measured during the sunlit part of about 14.5 sun-synchronous orbits per day. Trace gases, such as ozone (O_3), sulfur dioxide (SO_2) and nitrogen dioxide (NO_2), are retrieved from the reflectance spectra as well as cloud and aerosol properties.

The measurement principle is an along-track (push-broom) scanner with a swath width of 2600 km which is divided in 60 pixels. The ground pixel size varies between 13 km × 24 km at nadir and 40 km × 160 km at the swath edge. The spatial sensitivity

ACPD
14, 31039–31090, 2014

within a ground pixel is nearly constant in across-track direction but decreases in along-track direction.

2.2 Retrieval of tropospheric NO_2 column densities

The standard product (SP2) (Bucsela et al., 2006, 2013) is the basis for the HK NO_2 retrieval. Therefore, we give a brief introduction to their algorithm. The SP2 retrieval algorithm has three major steps:

1. The total slant column densities S are obtained from the reflectance spectra using the differential optical absorption spectroscopy (DOAS) technique (Platt and Stutz, 2008).
2. The stratospheric slant column densities S_{strat} are subtracted from the total column S using a stratosphere–troposphere separation (STS) algorithm (Bucsela et al., 2013).
3. The tropospheric slant column densities S_{trop} are converted to vertical column density V_{trop} using a tropospheric air mass factors (AMF) A_{trop} (Palmer et al., 2001).

The AMF is defined as the ratio of slant and vertical column density (Solomon et al., 1987). Thus the tropospheric column density V_{trop} is calculated by

$$V_{trop} = \frac{S - S_{strat}}{A_{trop}} = \frac{S_{trop}}{A_{trop}}. \quad (1)$$

The tropospheric AMF depends on parameters such as sun position, satellite position, surface reflectance, atmospheric scattering properties due to air molecules, aerosols and clouds, and the NO_2 profile shape. It is related to the vertical sensitiv-

ACPD
14, 31039–31090, 2014

ity of the satellite instrument and can be computed for N vertical layers by

$$A_{\text{trop}} = \frac{\sum_{k=1}^{N} \alpha_k \, m_k \, V_k}{\sum_{k=1}^{N} V_k} \tag{2}$$

with:

- α_k: an empirical temperature correction coefficient accounting for the temperature dependency of the NO_2 absorption cross section,
- m_k: the differential or box air mass factor which describes the instrument sensitivity for layer k,
- V_k: the partial NO_2 VCD of layer k.

The correction coefficient α_k can be computed by the empirical formula

$$\alpha_k = 1 - 0.003\,\text{K}^{-1}(T_k - T_{\text{ref}}) \tag{3}$$

where T_k is the temperature in layer k and T_{ref} is reference temperature of the NO_2 absorption cross section ($T_{\text{ref}} = 220\,\text{K}$) (Bucsela et al., 2013).

The box air mass factors m_k can be computed with a radiative transfer model. The SP2 algorithm uses the TOMRAD radiative transfer model (Dave, 1965). The AMF formulation used in SP2 is based on a AMF formulation by Palmer et al. (2001). In partly cloudy scenes, SP2 computes the box AMFs using the independent pixel approximation (IPA). The approximation calculates AMFs as weighted sums of a cloudy m_k^{cloudy} and a clear m_k^{clear} component:

$$m_k = w \cdot m_k^{\text{cloudy}} + (1 - w) \cdot m_k^{\text{clear}}, \tag{4}$$

where w is the aerosol/cloud radiance fraction (CRF), that is the fraction of measured radiation that results from clouds and aerosols (Acarreta et al., 2004).

ACPD
14, 31039–31090, 2014

The products $\alpha_k m_k$ are called scattering weights. They can be used to recalculate the AMF with different profile shapes which could be taken from a regional CTM.

In SP2, the partial VCD V_k are taken from the Global Modeling Initiative (GMI) CTM (Duncan et al., 2007; Strahan et al., 2007) which combines stratospheric chemistry described by Douglass et al. (2004) and tropospheric O_3-NO_x-hydrocarbon chemistry from the GEOS-Chem model (Bey et al., 2001). It should be noted that only the relative shape of the profile $n_k = V_k/V_{\text{trop}}$ is required for the AMF calculation.

Bucsela et al. (2013) estimated tropospheric NO_2 VCD uncertainties to be $1 \times 10^{15}\,\text{cm}^{-2}$ for clear skies and up to $3 \times 10^{15}\,\text{cm}^{-2}$ for large cloud radiance fractions. In polluted regions, the main uncertainties are in the DOAS fit (10 % relative error) and in the tropospheric AMFs (20–80 %).

2.3 SCIATRAN radiative transfer model

SCIATRAN is a one-dimensional RTM which can be used for the calculation of box AMFs (Rozanov et al., 2005). The model is designed as a forward model for the retrieval of atmospheric constituents from measurements of scattered light by satellite, ground or airborne instruments. The wavelength range goes from 175 to 2380 nm which includes the ultra violet, visible and near infra red part of the spectrum.

SCIATRAN solves the integro-differential radiative transfer equation using the discrete-ordinates method (DOM) in the plane-parallel or pseudo-spherical mode to calculate box AMF profiles. Box AMFs m_k are derived from weighting functions which describe the sensitivity of the reflectance spectrum R to a perturbation of a model parameter Δn in layer z_k. In SCIATRAN, weighting functions are computed by a quasi-analytic approach (Rozanov et al., 1998). If Δn is a perturbation of the NO_2 number density n_k, the box AMF m_k is the negative weighting function (Rozanov and Rozanov, 2010).

ACPD
14, 31039–31090, 2014

3 Methodology

In this section, we describe the RAQM network, the regional CTM run and the HK NO_2 retrieval. Our study period is from October 2006 to January 2007. This period was chosen because cloud fractions in the PRD region are lowest in this season and OMI measurements in later years are affected by a row anomaly which reduces the number of valid measurements. Details about the row anomaly can be found on http://www.knmi.nl/omi/research/product/rowanomaly-background.php.

3.1 Ground network

3.1.1 Meteorological observations

Meteorological observations were used for the evaluation of the simulated meteorological fields which were used to drive the CTM. The data were measured by three automatic weather stations in Hong Kong. The stations are at the Hong Kong Observatory (HKO) headquarters, at the Hong Kong International Airport (HKIA) near Tung Chung and on Waglan Island (WGL). The locations of the stations are shown by square markers in Fig. 1. The Hong Kong Observatory is in the city centre of Kowloon and surrounded by high buildings. The airport is located on an artificial island to the north of mountainous Lantau Island. Waglan Island is a small island located to the east of Hong Kong Island. The island is too small to be resolved by the model grid. The WGL station is located 56 m a.s.l. and used as background station by the Hong Kong Observatory. The meteorological parameters are hourly measurements of temperature (T), humidity (q), sea surface pressure (p) and wind (v). Temperature and humidity are measured at 2 m above ground level (a.g.l.).

3.1.2 Pearl River Delta Regional Air Quality Monitoring Network

Ground-level NO_2 mixing ratios were provided by the RAQM network. The network was established by the governments of the Guangdong province and Hong Kong to monitor

ACPD
14, 31039–31090, 2014

the air quality in the PRD region and has been in operation since 30 November 2005. It consists of sixteen automatic air quality monitoring stations (see Fig. 1, round markers). The network measures hourly NO_2, SO_2, O_3 and PM_{10}. The monitoring network was used to validate the NO_2 mixing ratios of the OMI NO_2 products and the CMAQ simulation. In the network, NO_2 was measured by chemiluminescence and DOAS technique with an accuracy and precision of about 10 % (GDEMC and HKEPD, 2006).

3.2 CMAQ model simulation

3.2.1 Model run

Three dimensional atmospheric chemistry was simulated in the PRD region for the study period. The simulations were performed with the CMAQ modelling system version 4.7.1 (Byun and Schere, 2006).

Three model domains were defined using a Lambert conformal conic projection (Fig. 1). The coarse domain (D1) covers East Asia with a spatial resolution of 27 km × 27 km. The nested domains have grid resolutions of 9 km × 9 km (D2) and 3 km × 3 km (D3), receptively.

Meteorological fields were provided by the Weather Research and Forecasting (WRF) modelling system (Skamarock et al., 2008) driven by NCEP Final Analysis (FNL) data (NCEP et. al., 1997). Horizontal advection was modelled by the mass-conserving YAMO scheme (Yamartino, 1993). The default vertical advection scheme was replaced with the WRF omega calculation with the piecewise parabolic method. The new scheme is the default scheme in CMAQ version 5 and is assumed to provide better vertical profiles. Accurate vertical profiles are important for satellite measurements of air pollutants.

The gas-phase chemistry was modelled by the Euler backward iterative solver optimized for the Carbon Bond-05 mechanism with chlorine (Yarwood et al., 2005). Aerosol chemistry was modelled by the fifth-generation CMAQ aerosol model (aero5) and the impact of clouds on deposition, mixing, photolysis, and aqueous chemistry was de-

ACPD
14, 31039–31090, 2014

scribed by the ACM cloud processor (Pleim and Chang, 1992). Three-dimensional extinction coefficients were computed by the empirical IMPROVE formula (Malm et al., 1994).

The emission inventory used in this simulation was compiled by Du (2008). The inventory combines monthly anthropogenic emission from INTEX-B (Zhang et al., 2009) with biogenic emissions from GEIA (Global Emissions Inventory Activity, Guenther et al., 1995), and biomass burning and ship emissions from TRACE-P (Streets et al., 2003). The INTEX-B emissions were updated with regional emissions for Hong Kong provide by the Hong Kong Environmental Protection Department (Du, 2008). The low-resolution emissions were spatially allocated to each grid cell based on geographic and socio-economic information as well as updated road network and land cover data. Furthermore, weekly and daily cycles were included to the emission inventory (Du, 2008).

3.2.2 Data processing

Model outputs are hourly ground level values and three-dimensional fields averaged from 13:00 to 15:00 LT (OMI overpass time).

In addition, at each ground stations, time series of hourly meteorological parameters and NO_2 mixing ratios were extracted from the model output. The surface pressure in the model was converted to sea level pressure using the simulated temperature. The wind vector in the model was taken at the height of the measurement stations to account for the elevation of the stations above averaged surface height.

Since OMI has a lower spatial resolution than CMAQ, the satellite instrument cannot resolve high-frequency features in the simulated NO_2 distribution. Therefore, the two datasets were made comparable by averaging the CMAQ data for each OMI ground pixel in an orbit. The pixel boundaries were provided by the overlapping ground pixel product. Within the boundaries, each grid point was weighted based on the instrument's spatial sensitivity (Dobber et al., 2006; Kurosu and Celarier, 2010). Since the set of averaged data is not conveniently visualisable, the CMAQ data were pro-

ACPD
14, 31039–31090, 2014

jected back onto a 0.01° × 0.01° longitude–latitude grid using a recently developed gridding algorithm (Kuhlmann et al., 2014). The gridding algorithm is available at: https://github.com/gkuhl/omi. In this step, missing OMI pixels were also removed from the CMAQ data. Using this approach, the NO_2 distributions of OMI and CMAQ are directly comparable.

3.3 The Hong Kong (HK) OMI NO_2 retrieval

For the HK NO_2 retrieval, we recalculated tropospheric AMFs by Eq. (2) with new ancillary parameters. The new AMFs were used to compute the tropospheric VCDs by Eq. (1).

For the AMF calculation, a set of ancillary parameters was put together for each OMI ground pixel. The parameters were taken mainly from the WRF/CMAQ simulation. Thus, the retrieval does not depend on any other CTM model which makes the model evaluation easier. The ancillary parameters are surface elevations, temperature, pressure and NO_2 profiles, and aerosol extinction coefficients. The model domain (D3, Fig. 1) has a spatial resolution of 3 km × 3 km. The WRF/CMAQ data were temporally averaged to the OMI overpass time. Further ancillary parameters are cloud height and aerosol/cloud radiance fraction (CRF), which were taken from the OMI O_2–O_2 cloud product (Acarreta et al., 2004), and surface reflectance, which was taken from the MODIS MCD43C2 black-sky albedo (BSA) product (Wanner et al., 1997; Lucht et al., 2000). Table 1 compares the updated parameters with the ancillary parameters used in SP2.

All ancillary parameters were projected to a 0.01° × 0.01° grid and then averaged to each OMI ground pixel. The grid points were weighted based on the instrument's spatial sensitivity within the pixel boundaries, in contrast to other regional retrievals, where each grid point was given equal weight (Russell et al., 2011; Lin et al., 2014).

We recalculated temperature correction coefficients $\alpha_k(T_k)$, box AMFs m_k and partial VCDs V_k. The temperature correction coefficients $\alpha_k(T_k)$ were calculated by the empirical Eq. (3) from the WRF/CMAQ output. The box AMFs were computed with the

ACPD
14, 31039–31090, 2014

SCIATRAN radiative transfer model. The partial VCDs were also calculated from the WRF/CMAQ output. As an example, two NO_2 profiles are shown in Fig. 2. In contrast to other regional retrievals, we used three-hour means instead of monthly means.

3.3.1 Surface reflectance

The surface reflectance was calculated from the MODIS MCD43C2 BSA product. The product is available every eight days compiled from 16 days of measurements. The spatial resolution is $0.05^\circ \times 0.05^\circ$ (Wanner et al., 1997; Lucht et al., 2000). We calculated the BSAs from the polynomial representation of the bidirectional reflectance distribution function (BRDF) using solar zenith angle (SZA) and model parameters for MODIS Band 3 (Lucht et al., 2000). MODIS Band 3 has a wavelength range from 459 to 479 nm and a centre wavelength of 470 nm. This band is closest to the DOAS fitting window used in the NO_2 retrieval (405–465 nm). Systematic errors due to the wavelength inconsistency are expected to be small. Over water, Lambertian equivalent reflectance (LER) has been reported to decrease from 440 to 470 nm (Kleipool et al., 2008; Zhou et al., 2010). We actually find increased BSA over water surfaces in the PRD region. The MODIS BSA has been used in other regional OMI NO_2 products (Zhou et al., 2010; Russell et al., 2011; Lin et al., 2014).

Since the BSA model parameters have missing values due to cloud contamination, Zhou et al. (2010) filled the data gaps by applying a series of spatial and temporal interpolations. They also reduced measurement noise by applying a smoothing filter. In this work, we combined their steps by using normalised convolution which is a useful algorithm for filling missing values (Knutsson and Westin, 1993). We used a three-dimensional, uniform kernel of size 5 to fill the gaps in the model parameters. To calculate the BSA for each OMI ground pixel, the interpolated BSA model parameters were also projected on the longitude–latitude grid.

ACPD
14, 31039–31090, 2014

3.3.2 Aerosols and clouds

Scattering by aerosols and clouds affects the AMF (Boersma et al., 2004; Lin et al., 2014). Aerosol scattering enhances the AMF, if aerosols are located below or at the same height as the NO_2 layer. On the other hand, aerosols scattering reduces the AMF, if aerosols are located above the NO_2 layer. In addition, aerosol optics affect the retrieval of cloud properties.

Clouds are typically handled by the independent pixel approximation (Eq. 4), while aerosols are treated only implicitly in all global and most regional NO_2 products. In SP2, cloud fraction and pressure are from the OMI O_2–O_2 cloud product which is sensitive to weakly absorbing aerosols (Boersma et al., 2011). Aerosols are also included by the OMI LER climatology which includes ground haze and persistent cloud features (Kleipool et al., 2008). Lin et al. (2014) included aerosols from a regional GEOS-Chem simulation. They used aerosol optical thickness (AOT) and assumed different profiles of aerosol extinction and absorption coefficients. They also recalculated the OMI cloud product to remove the aerosol component from the product. In a different study, Boersma et al. (2011) derived an empirical relationship between MODIS AOT and OMI aerosol/cloud fraction w:

$$w = 0.21 \cdot \mathrm{AOT}. \quad (5)$$

The formula was derived from cloud free observations over North America.

In our study, we treated clouds as in SP2 using the independent pixel approximation. In SCIATRAN, clouds were implemented as an opaque surface at the height of the OMI cloud pressure product with a surface reflectance of 0.8 and the box AMF was calculated with Eq. (4).

Aerosol extinction coefficients can be calculated from the CMAQ output using the empirical IMPROVE formula (Malm et al., 1994). By default, CMAQ calculates the ground level extinction coefficients. In the HK retrieval, we tested four different aerosol parametrizations:

ACPD
14, 31039–31090, 2014

Case 1: No explicit aerosol treatment, i.e. aerosols were only included implicitly through the OMI cloud product.

Case 2: Aerosols were described by the LOWTRAN aerosol parametrization which requires only very limited information about season, aerosols type, visibility and relative humidity at four different layers: planet boundary layer (PBL) (0–2 km), troposphere (2–10 km), stratosphere and mesosphere. We set the season to autumn/winter and the aerosol type to urban. The PBL visibility was calculated from the CMAQ ground extinction coefficients β using the definition of the meteorological optical range (MOR) (World Meteorological Organization, 2008):

$$\mathrm{MOR} = -\frac{\log 0.05}{\beta}. \quad (6)$$

The visibility in the free troposphere was set to 23 km. Furthermore, we assumed that no volcanic aerosols were in the stratosphere or mesosphere. The relative humidity in the PBL and the free troposphere were taken from WRF. Visibility and relative humidity were set to the nearest predefined value in the LOWTRAN parametrisation.

Case 3: Vertical profiles of extinction coefficients β were computed from CMAQ output using the IMPROVE formula. The formula includes a constant Rayleigh extinction coefficient of 0.01 which is subtracted to obtain the aerosol extinction coefficient β_{ext}. Since the IMPROVE formula calculates β_{ext} at 550 nm, an Ångström exponent α for urban aerosols is used to calculate extinction coefficients at 435 nm (Hess et al., 1998). Furthermore, a single scattering albedo ω_0 of 0.82 (urban aerosol) in PBL (below 2 km) and 0.93 in free troposphere is used to calculate aerosol absorption coefficients β_{abs}. The phase function is modelled by Henyey–Greenstein parametrisation with an asymmetry factor g of 0.689 (Hess et al., 1998). As examples, two β_{ext} profiles are shown in Fig. 2.

ACPD
14, 31039–31090, 2014

Case 4: Since this three parametrisations include aerosols implictly through the cloud product, aerosol might be counted twice. Therefore, the CRF was corrected by Eq. (5) using the AOT in CMAQ. This was done mainly because recalculation of the OMI cloud product was outside the scope of our study. Since this formula was derived from cloud free observations over North America, generalisation to cloudy pixels in other regions should be considered with great caution. Otherwise, aerosols were treated as in Case 3.

3.3.3 Application to OMI SP2

The ancillary parameters were used to calculate new AMFs for all OMI measurements within the PRD region. We created four NO_2 datasets (PRD-1 to PRD-4) for the four aerosol/cloud cases.

While OMI provides daily global coverage, the number of sufficient measurements, which allows for the study of the NO_2 distribution, is limited due to two factors. Firstly, the ground pixel size at the end of the swath is very large and thus not suitable for studying the local spatial distribution. Therefore, only the inner fifty out of sixty rows were used in this study. Secondly, the presence of clouds increases the retrieval uncertainty. Therefore, only ground pixels were used with aerosol/cloud radiance fractions smaller than 50 %. Since the CRF is also sensitive aerosol, this filter criterion is likely to remove heavily polluted days as well.

Based on these filtering constraints, orbits were picked which have a sufficient number of ground pixels to study the spatial distribution of NO_2 in PRD region. The orbits were projected onto a longitude–latitude grid using the same gridding algorithm which has been used to grid the CMAQ data (Kuhlmann et al., 2014).

At each ground stations, time series of NO_2 VCDs were extracted from the data. To study the additive and proportional differences, the OMI VCDs were converted to mixing ratios using the CMAQ NO_2 profile shapes. Since many stations are located on top of buildings, the mixing ratios were calculated at the station height using nearest-neighbour interpolation.

ACPD
14, 31039–31090, 2014

Finally, we used a standard set of typical ancillary parameters (Table 2) to study the impact of the ancillary parameters on the AMF and thus the NO_2 column densities.

4 Results and discussions

In this section, we demonstrate and discuss the results of our study. Firstly, we compare briefly the HK retrieval with SP2 to discuss the influence of the updated ancillary parameters. Secondly, we validate the WRF/CMAQ simulation using the RAQM network. Then, we validate the OMI datasets using the RAQM network. Finally, the OMI NO_2 datasets and CMAQ were compared to evaluate the regional chemistry transport model using the HK OMI NO_2 datasets.

4.1 OMI regional NO_2 product

In this subsection, we compare the global product (SP2) with our HK retrieval. Only difference relevant for the later discussion in this paper are described here. For a detailed discussion on the different ancillary parameters, we like to refer the reader to earlier studies and reference therein (Zhou et al., 2010; Russell et al., 2011; Lin et al., 2014).

In our study period, 56 days (46 % of all days) with sufficient OMI data were available. Two examples of ungridded NO_2 VCDs are shown in Fig. 3. The spatial distributions are similar for all products but differences can be seen in a pixel-by-pixel comparison. Particularly evident is that the NO_2 VCDs in the HK retrieval have larger maximum values than in the standard product.

The four-month mean NO_2 distributions are shown in Fig. 4c and e. The SP2 has a mean value of 0.4×10^{16} cm^{-2}. The mean values in the four datasets range from 0.6 to 0.7×10^{16} cm^{-2}. The smallest mean value has PRD-1 and the largest has PRD-2. PRD-3 and PRD-4 lie in between these extreme cases. The maximum value in the distribution of SP2 is about 3.5×10^{16} cm^{-2} while the HK retrieval datasets have maximum values ranging from 4.5–5.5 $\times 10^{16}$ cm^{-2}.

ACPD
14, 31039–31090, 2014

To study the difference without explicit aerosol treatment we compare SP2 and PRD-1. For this dataset, the VCDs are increased by (27 ± 39) %. The difference are due to the updated ancillary parameters, mainly surface reflectance and profile shapes, and thus due to the recalculated AMFs. For SP2, the mean AMF of all available pixels is 1.01 while the mean AMF of PRD-1 is about 17 % smaller (AMF = 0.83).

To quantify the impact of the high-resolution NO_2 profile shapes on the AMF calculation, we compare the CMAQ profiles with an annual GEOS-Chem profile ($2^\circ \times 2.5^\circ$ spatial resolution) which was used for a satellite validation study in Hong Kong (Chan et al., 2012). The profile was linearly interpolated and extrapolated to the CMAQ vertical levels. The three profiles (see Fig. 2) have been used to compute AMF for the standard case without aerosols (Table 2). The "polluted" CMAQ NO_2 profile has an AMF of 0.82 and is about 3 % smaller than the "clean" profile (AMF = 0.84). The GEOS-Chem profile has an AMF of 1.19 which is 41 % larger than the "clean" and 45 % larger than the "polluted" CMAQ profile. The difference results from the different relative profile shapes. In the CMAQ profiles, the NO_2 number density decreases with altitude, while the GEOS-Chem profile is nearly constant above 2 km. The different profile shapes are related to the different vertical advection schemes used in both models. We expect that the regional CMAQ model provides more accurate vertical distributions than the global GEOS-Chem model. The impact of uncertainties in the profile shapes is difficult to quantify because the uncertainties are not well known due to the lack of NO_2 profile measurements (Boersma et al., 2004). Therefore, we calculated a distribution of AMFs using the simulated profiles at each ground pixel using the standard case. The mean AMF is 0.89 with a SD of 0.08. The largest AMF is 1.64 as a result of an elevated NO_2 layer in the upper troposphere. The smallest AMF is 0.75 which is 16 % smaller than the mean AMF. The small AMF is the result of a heavily polluted ground layer. In summary, the AMF for the high-resolution profiles is about (35 ± 11) % smaller than the low-resolution profile.

The profile shapes can also be used to convert VCDs to number concentrations or mixing ratios. For the standard case, the mean conversion factor $(V_0/(\Delta z_0 V_{\text{trop}}))$

ACPD
14, 31039–31090, 2014

is $(1.47 \pm 0.47) \times 10^{-3}$ m^{-1} using all available profiles. Therefore, the uncertainty is about 32 %. The conversion factor of the "clean" and "polluted" profiles are 1.44 and 1.47×10^{-1} m^{-3}, respectively, which is a difference of about 3 %. The GEOS-Chem profile has a conversion factor 3.92×10^{-3} m^{-1} because of the different profile shape.

The impact of the surface reflectance can be quantified easier. The mean MODIS BSA is shown for a SZA of 48° in Fig. 5a. On average, the MODIS BSA is about 0.01 ± 0.02 smaller than the OMI LER (not shown). The BSA is smaller than LER over land but larger over water. The AMF sensitivity to uncertainties in the surface reflectance depends strongly on the surface reflectance itself (Fig. 6). For the mean surface reflectance (BSA = 0.05) the sensitivity is about 0.06. Therefore, the AMF is reduced by 5 to 10 % if the OMI LER product is replaced by MODIS BSA. To identify the improvement due to the higher spatial and temporal resolution, we averaged the BSA to the lower spatial resolution used in the global product (0.5° × 0.5°). Then, we subtracted the high-resolution BSA used in our regional product (Fig. 5b). The distribution shows areas with large differences (up to ±0.03) along the urbanised and likely polluted coastline. As a result, if we assume an AMF of 0.83, the retrieval error, due to a low spatial resolution, can be locally as large as 20 %.

The differences between PRD-1 to PRD-4 are due to the different aerosol treatments. Table 3 shows the AMFs for the different aerosol cases using the "clean" and "polluted" profiles in Fig. 2 and the standard parameters (Table 2). PRD-3 and PRD-4 are equal because the standard parameter assume cloud free conditions. If aerosols are included, the AMF is reduced because the aerosol is located above the NO_2 layer (Fig. 2).

In PRD-2, the ground level extinction coefficient is used as constant coefficient in the PBL (0–2 km). If PRD-2 is compared to PRD-1, the AMF is reduced by 19 % for the "clean" and by 57 % for the "polluted" aerosol profile (Table 3). The β_{ext} profiles in Fig. 2 show that using the ground level extinction coefficient is reasonable for a "clean" b_{ext} profile but not for a "polluted" profile. In the latter case, β_{ext} would be overestimated between 1 and 2 km and thus reduce the AMF because these aerosols are located

ACPD
14, 31039–31090, 2014

above the NO_2 layer. As consequence, the ground level extinction coefficient should not be used as PBL mean value for "polluted" cases, because this assumption can severely overestimate the NO_2 column densities.

PRD-3 and PRD-4 use a b_{ext} profile calculated with the IMPROVE formula. The b_{ext} profiles have a maximum value at about 500 m above ground which correlates with the maximum relative humidity. The shape of the profiles is in reasonable agreement with LIDAR measurements in Hong Kong (He et al., 2008). However, the formula was not developed to calculate profiles in an urban environment and thus should be treated with caution. If PRD-3 is compared to PRD-1, the AMF is reduced between 8 and 14 % (Table 3).

If aerosols are included, PRD-4 is likely to be the most reasonable assumption. The mean difference between NO_2 VCDs in SP2 and PRD-4 is (+31 ± 38) %. The difference between PRD-1 and PRD-4 is (+4 ± 11) % showing a large impact due to aerosols. The difference between PRD-4 and PRD-3 is (+1 ± 7) %.

To conclude, our regional datasets have higher NO_2 VCDs than the global product (SP2) because of updated ancillary parameters. On the local scale, systematic errors should be reduced because of the higher spatial resolution.

4.2 WRF/CMAQ validation with ground measurements

In this section, the WRF/CMAQ model is evaluated with ground measurements of meteorological observations and the PRD RAQM network. The errors measures used on the validation are summarised in the appendix.

4.2.1 Temperature, humidity, pressure and wind

The results of the validation are shown in the Supplement. The index of agreement (IOA, see Appendix A) between observed and simulated sea level pressure is high (IOA = 0.99) at all stations. Simulated temperature and humidity also agree well with the observations. The model slightly underestimates temperature and humidity over

ACPD
14, 31039–31090, 2014

land (HKO and HKIA). The model also overestimates humidity on Waglan Island where the model data are at the sea surface while measurements were taken at station height of 56 m over the sea surface.

Since the wind field is impacted strongly by local topography, the agreement between model and observation is normally lower where the topography is complex and thus cannot be resolved by the model. The Hong Kong Observatory uses Waglan Island as reference station because it is not influenced by local topography. The agreement between model and observations on Waglan Island is good (IOA = 0.84). At HKIA the wind field is impacted by the mountainous Lantau Island and thus the agreement is lower (IOA = 0.68). The HKO station is located within urbanised Kowloon and surrounded by high buildings. Consequently, the agreement between model and observations is low (IOA = 0.57).

The evaluation of the meteorological fields shows good agreement between model and observations within the expected limitations due to the model resolution. The agreement is lower for the wind fields due to the impact of local topography. Unfortunately no meteorological data for the whole PRD region were available for this analysis. However, due to the high agreement in Hong Kong, similar model performance is expected in the complete model domain. The meteorological fields are sufficient to provide input for the chemistry transport simulations.

4.2.2 NO_2 mixing ratios

The results of the statistical evaluation between CMAQ and RAQM network are summarised in the Supplement. At the sixteen stations, the index of agreements vary between 0.29 and 0.75. At most stations the IOA is about 0.5. At Tap Mun, the low IOA is the result of several peaks in the simulated time series which are not found in the measurements. The peaks were traced back to NO_x emissions at the Dapend Peninsula about 15 km east of Tap Mun (not shown). Other stations in Hong Kong have IOA above average.

ACPD
14, 31039–31090, 2014

There are various reasons for the disagreement between model and measurements. Firstly, the point measurement may not be representative for the grid cell because of the influence of local sources and sinks. Secondly, local topography and station height can also impact the NO_2 mixing ratios. On the other hand, the differences can arise from the model due to the limited parametrisation of the chemistry and in particular the insufficient knowledge of the strength and distribution of the emissions.

The average ground mixing ratios are shown in Fig. 7. In the observations, two major plumes can be identified at Hong Kong and Shenzhen (HK & SZ), which includes the network stations Liyuan, Tap Mun, Tung Chung and Tsuen Wan, and Foshan and Guangshou (FS & GZ), which includes the stations Huijingcheng, Luhu Park, Shunde Dangxioa and Wanqingsha. The latter plume cannot be found in the simulations. The mean bias is close to zero (−5 %) at the stations in HK & SZ. The bias is larger in FS & GZ with a MB of −17.6 ppbv (−45 %).

The better agreement over Hong Kong is thought to be the result of the updated emission inventory with local information from Hong Kong which are more accurate. The low agreement between model and observation is not very satisfying. In another study, Wu et al. (2012) evaluated CMAQ in the PRD region using a similar emission inventory and reported similar CVs (see Appendix A for definition) and normalised mean biases. The low model performance can impact the quality of the OMI NO_2 dataset because the low model performance might reduce the accuracy of the NO_2 profile shape and thus impact the air mass factor and the conversion factor which is used to convert VCDs to ground mixing ratios.

4.3 OMI validation with ground measurements

In this subsection, OMI NO_2 columns were compared with the RAQM network. The validation with point measurements is challenging, because OMI measures the mean value within the ground pixels (at least 13 km × 24 km). Since NO_2 has a high spatial variability, area average and point measurement may not agree well; in particular in an urban area with complex NO_2 sources and sinks. Furthermore, if the VCDs are

ACPD
14, 31039–31090, 2014

converted to ground values with the CMAQ profile shapes, the validation depends on the modelled NO_2 profiles which can have large uncertainties.

In order to get an idea for the expected deviations, we compared the time series of the processed CMAQ data, which have been averaged to the OMI ground pixels, with the raw CMAQ data (3 km × 3 km) at the 16 stations. Table 4 shows the mean error measures for all stations and for the stations within the two plumes. The correlation coefficient is low, in particular, over HK & SZ. This lower agreement in Hong Kong could result from the complex terrain along the coastline and the strong gradient between clean and polluted air (see Fig. 7a). Against that, the NO_2 distribution in FS & GZ is smoother. Table 4 also shows that the processed data have lower mixing ratios with a mean bias between −10 and −20 % which is the result of the spatial averaging. The generalisation of these results to the OMI validation should be done with caution because it requires that the model simulates the spatial distribution on a small scale accurately. Nonetheless, this analysis provides some useful information on the expected deviations between satellite and ground measurements.

To study additive and proportional differences between satellite and ground measurements, the OMI VCDs were converted to ground level mixing ratios using the CMAQ NO_2 profile shapes. As an example, the ground mixing ratio distribution for 29 January 2007 is shown in Fig. 8 using a "standard" and the newly developed gridding algorithm. The new algorithm creates continuous distributions which is helpful for the study of the spatial distribution distribution. It should be noted that the high-resolution features are the result of modelled profile shapes. Therefore, the ground mixing ratios depend strongly on the NO_2 profile shape in the model.

Table 5 shows the statistical measures for the comparison between OMI and the ground network for SP2 and datasets using the HK retrieval. The correlation coefficients are similar for all datasets. The size of the correlation coefficient is comparable to the expected values (Table 4). The correlation coefficients is slightly smaller at FS & GZ which is likely related to the low model performance in this area.

ACPD
14, 31039–31090, 2014

There are large differences between the mean biases. The bias is largest for the global product (SP2). In the HK retrieval, the mean bias depends on the amount of aerosols. The bias is largest for PRD-1 and smallest for PRD-2, while PRD-3 and 4 lie in between them. The magnitude of the bias is closest to the expected value for PRD-4. The reduced mean bias is an important improvement of the HK NO_2 retrieval.

Table 6 shows the mean values of CMAQ, OMI datasets and RAQM network at the location of the 16 stations. If the local NO_2 distribution was simulated perfectly, the raw CMAQ data would agree with the network measurements and the processed CMAQ data would agree with the OMI measurements. However, the bias between OMI PRD-4 and RAQM network at FS & GZ is larger than the expected value. The difference is likely the result of the CMAQ model bias in this area. If we compare the "clean" and "polluted" standard case (Table 2), the different profile shape (−3 %), conversion factor (−3 %) and the influence of the aerosols (−10 %) can increase the AMF by 10 to 20 % (see Sect. 4.1). As a result, the OMI NO_2 VCDs would be larger and the bias between OMI and network would become smaller.

To conclude, the correlation coefficient between all OMI datasets and ground measurements is low. The low correlation is mainly related to the OMI ground pixel size as well as to the unsatisfactory performance of the CMAQ model. However, the HK retrieval reduces the mean bias between satellite and ground measurements significantly. The larger bias in FS & GZ suggests that OMI VCDs might be still underestimated in the HK retrieval (PRD-4) due to the model bias in this region.

4.4 CMAQ evaluation with OMI NO_2 datasets in the model domain

In this subsection, we compare the OMI datasets with the CMAQ data. We discuss mainly PRD-4 which performed best in the validation with ground measurements. Since the correlation between OMI and RAQM network is low, only spatially or temporally averaged distribution were compared which reduces the random noise.

Figure 4a–c and e shows the four-month averaged CMAQ and OMI NO_2 VCDs. The averaged raw CMAQ data and the processed CMAQ data are shown Fig. 4a and b.

ACPD
14, 31039–31090, 2014

Some high-resolution features, which cannot be resolved by OMI, are smoothed in the processed NO_2 distribution. Since the OMI lattice changes with each orbit, this processing also provides an easy way to distinguish features which can and cannot be resolved by the current orbit.

The differences between CMAQ and OMI are shown in Fig. 4d and f. The two major plumes at Foshan and Guangzhou (FS & GZ) and Hong Kong and Shenzhen (HK & SZ) are marked by the left and right box, respectively. For each orbit, OMI and CMAQ VCDs were averaged within the two boxes to create a time series for each plume. The results of the time series analysis are shown in Table 7 and two scatter plots are shown in Fig. 9.

At FS & GZ, the correlation coefficient is low ($r \approx 0.4$) and the CMAQ VCDs are much smaller than the OMI PRD-4 VCDs (MB = −40 %). At HK & SZ, the correlation is better ($r \approx 0.6$) and the CMAQ VCDs are larger than the OMI VCDs (+15 %). These results confirm the CMAQ bias identified in the evaluation with the ground measurements. The model biases between OMI PRD-4 and CMAQ (processed) are consistent with the biases found between RAQM network and CMAQ (raw) (see Table 6). Since the CMAQ distribution has been processed like OMI, no area averaging effects occur in this comparison. The errors in the OMI measurements are mainly due to uncertainties in the ancillary parameters which are mainly taken from the model simulation.

The HK retrieval can be used for the study of the spatial NO_2 distribution. An example is the shape of the plume at Hong Kong. In CMAQ, the plume has an elliptic shape with a strong, south-western outflow. In the OMI datasets, this feature is less distinct. This difference might be caused by the spatial resolution of CMAQ which does not resolve the mountainous Lantau Island (south of Tung Chung, see Fig. 1).

The OMI measurements can also be used where no ground measurements are available. For example, the OMI measurements show several smaller plumes which are missing in CMAQ. For instance, in the northern and western part of the model domain.

In summary, the HK retrieval provides a better suited dataset which can be used for the evaluation of the CMAQ model.

ACPD
14, 31039–31090, 2014

5 Discussions and conclusions

In this paper, we evaluate a regional CTM (3 km × 3 km spatial resolution) with satellite measurements. We simulated three-dimensional atmospheric chemistry with the CMAQ modelling system the PRD region from October 2006 to January 2007. Furthermore, we developed a new OMI NO_2 retrieval for this region. The CMAQ model was evaluated with the global OMI NO_2 standard product (SP2), our HK NO_2 retrieval using different aerosol parametrizations (PRD-1 to PRD-4), and ground measurements of the PRD Regional Air Quality Monitoring (RAQM) network.

In the HK retrieval, we recalculated tropospheric AMFs using updated ancillary parameters of NO_2 profile shapes, surface reflectance and aerosol profiles. Our best retrieval (PRD-4) increases the NO_2 VCDs by (+31 ± 38) %, when compared to SP2, and thus reduces the mean bias between satellite and ground measurements significantly (−15 % instead of −41 %). The differences are due to changes in the ancillary parameters used for the AMF calculation. These parameters are NO_2 profile shapes (−35 ± 11) %, surface reflectance (−5 to −10 %) and aerosols (−8 to 14 %). The remaining difference between satellite and ground measurements can be explained by the area averaging due to the OMI ground pixel size and by the CMAQ model bias because the OMI NO_2 retrieval depends on the CMAQ model output. As a result, if the CMAQ model underestimates NO_2 mixing ratios or aerosols, the OMI VCDs can be underestimated as well. This relation should be considered in an evaluation study.

In a polluted environment, accurate knowledge of the vertical profiles of aerosol and cloud scattering as well as NO_2 profile shapes are important to calculate accurate column densities. Our study is limited by unquantified errors due to uncertainties in the NO_2 profile and aerosol profile. In future studies, the HK retrieval should be reviewed by validating the CMAQ NO_2 profiles. Furthermore, the aerosol optical properties were calculated by the IMPROVE formula which has not been developed to calculate profiles in an urban environment. However, the IMPROVE formula can be improved for such an application (Zhang et al., 2013) which we like to include in a future version.

ACPD
14, 31039–31090, 2014

Otherwise, optical properties can be calculated by Mie theory. The aerosol information can be improved further by validating them with ground- or satellite-based products. A third aspect is the impact of clouds which need to be studied more in future. Satellite products, which provide a clean separation between aerosols, clouds and surface reflectance, are desirable, because this would allow to use different data sources for these ancillary parameters.

The performance of the model is not very satisfying. The correlation between CMAQ and RAQM network is low ($r \approx 0.3$) and the model underestimates the NO_2 concentrations in the north-western model domain (Foshan and Guangzhou). The low performance is assumed to be associated with the used emissions inventory, because the model performance is better in Hong Kong and Shenzhen where the emission inventory has been updated with local data. The model evaluation with the HK retrieval (PRD-4) gives similar results. In Hong Kong and Shenzhen, the model overestimates the NO_2 VCDs by about 15 %, while the correlation coefficient is satisfactory ($r = 0.56$). In Foshan and Guangzhou, the correlation is low ($r = 0.37$) and the model underestimates the VCDs strongly (MB = −40 %). Furthermore, we estimated that the HK retrieval also underestimated VCDs by about 10 to 20 % in Foshan and Guangzhou because of the influence of the model parameters on the AMF. The results of both model evaluations with the RAQM network and the datasets created by the HK algorithm are consistent.

To conclude, our study demonstrates that the datasets created by the HK retrieval are suitable for the evaluation of the spatial distribution and the magnitude of NO_2 concentrations in the model. We showed that a retrieval, which updates not only the profile shapes, reduces the OMI bias over urban areas. In future studies, easy-to-use tools need to be developed which allow such evaluations of CTMs with satellite measurements as easy as using ground network measurements.

Appendix A: Error measures

The following measures are used to compare observations and model:

ACPD
14, 31039–31090, 2014

– Index of agreement (Willmott, 1981):

$$\mathrm{IOA} = 1 - \frac{\sum_{i=1}^{N}(x_i - y_i)^2}{\sum_{i=1}^{N}(|x_i - \langle y\rangle| + |y_i - \langle y\rangle|)^2} \quad \text{(A1)}$$

where $\langle\cdot\rangle$ is the mean value.

– Pearson's correlation coefficient:

$$r = \frac{1}{n-1}\sum_{i=1}^{N}\left(\frac{y_i - \langle y\rangle}{\sigma_y}\right)\left(\frac{x_i - \langle x\rangle}{\sigma_x}\right) \quad \text{(A2)}$$

σ_x and σ_y are sample SDs.

– Root mean square error:

$$\mathrm{RMSE} = \sqrt{\frac{1}{N}\sum_{i=1}^{N}(x_i - y_i)^2}. \quad \text{(A3)}$$

– Coefficient of variation of the RMSE:

$$\mathrm{CV} = \frac{\mathrm{RMSE}}{\langle y\rangle}. \quad \text{(A4)}$$

– Mean bias:

$$\mathrm{MB} = \frac{1}{N}\sum_{i=1}^{N}(x_i - y_i). \quad \text{(A5)}$$

– Normalised mean bias:

$$\mathrm{NMB} = \frac{\mathrm{MB}}{\langle y\rangle}. \quad \text{(A6)}$$

ACPD
14, 31039–31090, 2014

The Supplement related to this article is available online at doi:10.5194/acpd-14-31039-2014-supplement.

Acknowledgements. The work described in this paper is partly funded by the Guy Carpenter Asia-Pacific Climate Impact Centre (project no. 9360126), a grant from the Research Grant Council of Hong Kong (project no. 102912) and the start-up grant from City University of Hong Kong (project no. 7200296).

References

Acarreta, J. R., De Haan, J. F., and Stammes, P.: Cloud pressure retrieval using the O_2-O_2 absorption band at 477 nm, J. Geophys. Res., 109, D05204, doi:10.1029/2003JD003915, 2004. 31043, 31046, 31051

Bey, I., Jacob, D. J., Yantosca, R. M., Logan, J. A., Field, B. D., Fiore, A. M., Li, Q., Liu, H. Y., Mickley, L. J., and Schultz, M. G.: Global modeling of tropospheric chemistry with assimilated meteorology: model description and evaluation, J. Geophys. Res., 106, 23073–23095, doi:10.1029/2001JD000807, 2001. 31047

Boersma, K. F., Eskes, H. J., and Brinksma, E. J.: Error analysis for tropospheric NO_2 retrieval from space, J. Geophys. Res., 109, D04311, doi:10.1029/2003JD003962, 2004. 31053, 31057

Boersma, K. F., Eskes, H. J., Meijer, E. W., and Kelder, H. M.: Estimates of lightning NO_x production from GOME satellite observations, Atmos. Chem. Phys., 5, 2311–2331, doi:10.5194/acp-5-2311-2005, 2005. 31043

Boersma, K. F., Eskes, H. J., Veefkind, J. P., Brinksma, E. J., van der A, R. J., Sneep, M., van den Oord, G. H. J., Levelt, P. F., Stammes, P., Gleason, J. F., and Bucsela, E. J.: Near-real time retrieval of tropospheric NO_2 from OMI, Atmos. Chem. Phys., 7, 2103–2118, doi:10.5194/acp-7-2103-2007, 2007. 31041, 31042

Boersma, K. F., Eskes, H. J., Dirksen, R. J., van der A, R. J., Veefkind, J. P., Stammes, P., Huijnen, V., Kleipool, Q. L., Sneep, M., Claas, J., Leitão, J., Richter, A., Zhou, Y., and Brunner, D.: An improved tropospheric NO_2 column retrieval algorithm for the Ozone Monitoring Instrument, Atmos. Meas. Tech., 4, 1905–1928, doi:10.5194/amt-4-1905-2011, 2011. 31042, 31053

ACPD
14, 31039–31090, 2014

Bovensmann, H., Burrows, J. P., Buchwitz, M., Frerick, J., Noël, S., Rozanov, V. V., Chance, K. V., and Goede, A. P. H.: SCIAMACHY: mission objectives and measurement modes, J. Atmos. Sci., 56, 127–150, 1999. 31041

Bucsela, E. J., Celarier, E. A., Wenig, M. O., Gleason, J. F., Veefkind, J. P., Boersma, K. F., and Brinksma, E. J.: Algorithm for NO_2 vertical column retrieval from the ozone monitoring instrument, IEEE T. Geosci. Remote, 44, 1245–1258, doi:10.1109/TGRS.2005.863715, 2006. 31041, 31045

Bucsela, E. J., Krotkov, N. A., Celarier, E. A., Lamsal, L. N., Swartz, W. H., Bhartia, P. K., Boersma, K. F., Veefkind, J. P., Gleason, J. F., and Pickering, K. E.: A new stratospheric and tropospheric NO_2 retrieval algorithm for nadir-viewing satellite instruments: applications to OMI, Atmos. Meas. Tech., 6, 2607–2626, doi:10.5194/amt-6-2607-2013, 2013. 31041, 31045, 31046, 31047

Burrows, J. P., Weber, M., Buchwitz, M., Rozanov, V., Ladstätter-Weißenmayer, A., Richter, A., DeBeek, R., Hoogen, R., Bramstedt, K., Eichmann, K. U., Eisinger, M. and Perner, D.: The global ozone monitoring experiment (GOME): mission concept and first scientific results, J. Atmos. Sci., 56, 151–175, 1999. 31041

Byun, D. and Schere, K. L.: Review of the governing equations, computational algorithms, and other components of the Models-3 Community Multiscale Air Quality (CMAQ) modeling system, Appl. Mech. Rev., 59, 51–57, doi:10.1115/1.2128636, 2006. 31043, 31049

Callies, J., Corpaccioli, E., Eisinger, M., Hahne, A., and Lefebvre, A.: GOME-2 – Metop's second-generation sensor for operational ozone monitoring, ESA Bull.-Eur. Space, 102, 28–36, 2000. 31041

Chan, K. L., Pöhler, D., Kuhlmann, G., Hartl, A., Platt, U., and Wenig, M. O.: NO_2 measurements in Hong Kong using LED based long path differential optical absorption spectroscopy, Atmos. Meas. Tech., 5, 901–912, doi:10.5194/amt-5-901-2012, 2012. 31057

Dave, J. V.: Multiple scattering in a non-homogeneous, Rayleigh atmosphere, J. Atmos. Sci., 22, 273–279, 1965. 31046

Dobber, M., Dirksen, R., Levelt, P., Van den Oord, G. H. J., Voors, R., Kleipool, Q., Jaross, G., Kowalewski, M., Hilsenrath, E., Leppelmeier, G., de Vries, J., Dierssen, W., and Rozemeijer, N.: Ozone monitoring instrument calibration, IEEE T. Geosci. Remote, 44, 1209–1238, doi:10.1109/TGRS.2006.869987, 2006. 31050

ACPD
14, 31039–31090, 2014

Douglass, A. R., Stolarski, R. S., Strahan, S. E., and Connell, P. S.: Radicals and reservoirs in the GMI chemistry and transport model: comparison to measurements, J. Geophys. Res., 109, D16302, doi:10.1029/2004JD004632, 2004. 31047

Driscoll, C. T., Lawrence, G. B., Bulger, A. J., Butler, T. J., Cronan, C. S., Eagar, C., Lambert, K. F., Likens, G. E., Stoddard, J. L., and Weathers, K.: Acidic deposition in the northeastern United States: sources and inputs, ecosystem effects, and management strategies, Bioscience, 51, 180–198, doi:10.1641/0006-3568(2001)051[0180:ADITNU]2.0.CO;2, 2001. 31041

Du, Y.: New consolidation of emission and processing for air quality modeling assessment in Asia, Master's thesis, University of Tennessee, available at: http://trace.tennessee.edu/utk_gradthes/372 (last access: August 2014), 2008. 31050

Duncan, B. N., Strahan, S. E., Yoshida, Y., Steenrod, S. D., and Livesey, N.: Model study of the cross-tropopause transport of biomass burning pollution, Atmos. Chem. Phys., 7, 3713–3736, doi:10.5194/acp-7-3713-2007, 2007. 31047

Eskes, H. J. and Boersma, K. F.: Averaging kernels for DOAS total-column satellite retrievals, Atmos. Chem. Phys., 3, 1285–1291, doi:10.5194/acp-3-1285-2003, 2003. 31043

Guangdong Provincial Environmental Protection Monitoring Centre (GDEMC) and Environmental Protection Department, HKSAR (HKEPD): Pearl River Delta Regional Air Quality Monitoring Network – a report of monitoring results in 2006 (PRDAIR-2006-2), available at: http://www.epd.gov.hk/epd/english/resources_pub/publications/m_report.html (last access: April 2014), 2006. 31049

Guenther, A., Hewitt, C. N., Erickson, D., Fall, R., Geron, C., Graedel, T., Harley, P., Klinger, L., Lerdau, M., Mckay, W. A., Pierce, T., Scholes, B., Steinbrecher, R., Tallamraju, R., Taylor, J., and Zimmerman, P.: A global model of natural volatile organic compound emissions, J. Geophys. Res., 100, 8873–8892, doi:10.1029/94JD02950, 1995. 31050

Haagen-Smit, A. J.: Chemistry and physiology of Los Angeles smog, Ind. Eng. Chem., 44, 1342–1346, 1952. 31041

Han, K. M., Lee, C. K., Lee, J., Kim, J., and Song, C. H.: A comparison study between model-predicted and OMI-retrieved tropospheric NO_2 columns over the Korean peninsula, Atmos. Environ., 45, 2962–2971, doi:10.1016/j.atmosenv.2010.10.016, 2011. 31043

He, Q., Li, C., Mao, J., Lau, A. K.-H., and Chu, D. A.: Analysis of aerosol vertical distribution and variability in Hong Kong, J. Geophys. Res., 113, D14211, doi:10.1029/2008JD009778, 2008. 31059

ACPD
14, 31039–31090, 2014

Herron-Thorpe, F. L., Lamb, B. K., Mount, G. H., and Vaughan, J. K.: Evaluation of a regional air quality forecast model for tropospheric NO_2 columns using the OMI/Aura satellite tropospheric NO_2 product, Atmos. Chem. Phys., 10, 8839–8854, doi:10.5194/acp-10-8839-2010, 2010. 31043

Hess, M., Koepke, P., and Schult, I.: Optical properties of aerosols and clouds: the software package OPAC, B. Am. Meteorol. Soc., 79, 831–844, 1998. 31054

Kleipool, Q. L., Dobber, M. R., de Haan, J. F., and Levelt, P. F.: Earth surface reflectance climatology from 3 years of OMI data, J. Geophys. Res., 113, D18308, doi:10.1029/2008JD010290, 2008. 31052, 31053

Knutsson, H. and Westin, C.-F.: Normalized and differential convolution: methods for interpolation and filtering of incomplete and uncertain data, in: Proceedings of Computer Vision and Pattern Recognition ('93), New York City, USA, 16–19 June 1993, 515–523, 1993. 31052

Kuhlmann, G., Hartl, A., Cheung, H. M., Lam, Y. F., and Wenig, M. O.: A novel gridding algorithm to create regional trace gas maps from satellite observations, Atmos. Meas. Tech., 7, 451–467, doi:10.5194/amt-7-451-2014, 2014. 31051, 31055, 31089

Kurosu, T. P. and Celarier, E. A.: OMIPIXCOR Readme File, available at: http://disc.sci.gsfc.nasa.gov/Aura/data-holdings/OMI/documents/v003/OMPIXCOR_README_V003.pdf (last access: August 2014), 2010. 31050

Levelt, P., van den Oord, G., Dobber, M., Malkki, A., Visser, H., de Vries, J., Stammes, P., Lundell, J., and Saari, H.: The ozone monitoring instrument, IEEE T. Geosci. Remote, 44, 1093–1101, doi:10.1109/TGRS.2006.872333, 2006. 31041, 31044

Lin, J.-T., Martin, R. V., Boersma, K. F., Sneep, M., Stammes, P., Spurr, R., Wang, P., Van Roozendael, M., Clémer, K., and Irie, H.: Retrieving tropospheric nitrogen dioxide from the Ozone Monitoring Instrument: effects of aerosols, surface reflectance anisotropy, and vertical profile of nitrogen dioxide, Atmos. Chem. Phys., 14, 1441–1461, doi:10.5194/acp-14-1441-2014, 2014. 31042, 31051, 31052, 31053, 31056

Lucht, W., Schaaf, C., and Strahler, A.: An algorithm for the retrieval of albedo from space using semiempirical BRDF models, IEEE T. Geosci. Remote, 38, 977–998, doi:10.1109/36.841980, 2000. 31044, 31051, 31052

Malm, W., Gebhart, K., Molenar, J., Cahill, T., Eldred, R., and Huffman, D.: Examining the relationship between atmospheric aerosols and light extinction at Mount Rainier and North Cascades National Parks, Atmos. Environ., 28, 347–360, doi:10.1016/1352-2310(94)90110-4, 1994. 31050, 31053

ACPD
14, 31039–31090, 2014

National Centers for Environmental Prediction/National Weather Service/NOAA/U.S. Department of Commerce: NCEP FNL operational model global tropospheric analyses, April 1997 to June 2007, available at: http://rda.ucar.edu/datasets/ds083.0/ (last access: December 2013), 1997. 31049

Palmer, P. I., Jacob, D. J., Chance, K., Martin, R. V., Robert, J. D., Kurosu, T. P., Bey, I., Yantosca, R., Fiore, A., and Li, Q.: Air mass factor formulation for spectroscopic measurements from satellites: application to formaldehyde retrievals from the global ozone monitoring experiment, J. Geophys. Res., 106, 14539–14550, doi:10.1029/2000JD900772, 2001. 31045, 31046

Platt, U. and Stutz, J.: Differential Optical Absorption Spectroscopy: Principles and Applications, Springer Verlag, Berlin Heidelberg, 2008. 31045

Pleim, J. E. and Chang, J. S.: A non-local closure model for vertical mixing in the convective boundary layer, Atmos. Environ., 26, 965–981, doi:10.1016/0960-1686(92)90028-J, 1992. 31050

Rozanov, A., Rozanov, V., Buchwitz, M., Kokhanovsky, A., and Burrows, J.: SCIATRAN 2.0 – a new radiative transfer model for geophysical applications in the 175–2400 nm spectral region, Adv. Space Res., 36, 1015–1019, 2005. 31047

Rozanov, V., Kurosu, T., and Burrows, J.: Retrieval of atmospheric constituents in the uv-visible: a new quasi-analytical approach for the calculation of weighting functions, J. Quant. Spectrosc. Ra., 60, 277–299, doi:10.1016/S0022-4073(97)00150-7, 1998. 31047

Rozanov, V. V. and Rozanov, A. V.: Differential optical absorption spectroscopy (DOAS) and air mass factor concept for a multiply scattering vertically inhomogeneous medium: theoretical consideration, Atmos. Meas. Tech., 3, 751–780, doi:10.5194/amt-3-751-2010, 2010. 31047

Russell, A. R., Perring, A. E., Valin, L. C., Bucsela, E. J., Browne, E. C., Wooldridge, P. J., and Cohen, R. C.: A high spatial resolution retrieval of NO_2 column densities from OMI: method and evaluation, Atmos. Chem. Phys., 11, 8543–8554, doi:10.5194/acp-11-8543-2011, 2011. 31042, 31051, 31052, 31056

Skamarock, W. C., Klemp, J. B., Dudhia, J., Gill, D. O., Barker, D. M., Duda, M. G., Huang, X.-Y., Wang, W., and Powers, J. G.: A description of the advanced research WRF Version 3, National Center for Atmospheric Research, Boulder, Colorado, USA, NCAR/TN-475+STR, doi:10.5065/D68S4MVH, 2008. 31049

ACPD
14, 31039–31090, 2014

Solomon, S., Schmeltekopf, A., and Sanders, R.: On the interpretation of zenith sky absorption measurements, J. Geophys. Res., 92, 8311–8319, doi:10.1029/JD092iD07p08311, 1987. 31045

Strahan, S. E., Duncan, B. N., and Hoor, P.: Observationally derived transport diagnostics for the lowermost stratosphere and their application to the GMI chemistry and transport model, Atmos. Chem. Phys., 7, 2435–2445, doi:10.5194/acp-7-2435-2007, 2007. 31047

Streets, D. G., Bond, T. C., Carmichael, G. R., Fernandes, S. D., Fu, Q., He, D., Klimont, Z., Nelson, S. M., Tsai, N. Y., Wang, M. Q., Woo, J.-H., and Yarber, K. F.: An inventory of gaseous and primary aerosol emissions in Asia in the year 2000, J. Geophys. Res., 108, 8809, doi:10.1029/2002JD003093, 2003. 31050

Wanner, W., Strahler, A. H., Hu, B., Lewis, P., Muller, J.-P., Li, X., Schaaf, C. L. B., and Barnsley, M. J.: Global retrieval of bidirectional reflectance and albedo over land from EOS MODIS and MISR data: theory and algorithm, J. Geophys. Res., 102, 17143–17161, doi:10.1029/96JD03295, 1997. 31044, 31051, 31052

Willmott, C. J.: On the validation of models, Phys. Geogr., 2, 184–194, http://www.tandfonline.com/doi/abs/10.1080/02723646.1981.10642213, 1981. 31067

World Meteorological Organization: WMO Guide to Meteorological Instruments and Methods of Observation, World Meteorological Organization, 7th edn., Geneva, 2008. 31054

Wu, Q., Wang, Z., Chen, H., Zhou, W., and Wenig, M.: An evaluation of air quality modeling over the Pearl River Delta during November 2006, Meteorol. Atmos. Phys., 116, 113–132, doi:10.1007/s00703-011-0179-z, 2012. 31061

Yamartino, R. J.: Nonnegative, conserved scalar transport using grid-cell-centered, spectrally constrained Blackman cubics for applications on a variable-thickness mesh, Mon. Weather Rev., 121, 753–763, doi:10.1175/1520-0493(1993)121<0753:NCSTUG>2.0.CO;2, 1993. 31049

Yarwood, G., Rao, S., Yocke, M., and Whitten, G. Z.: Updates to the Carbon Bond chemical mechanism: CB05. Final Report to the U.S. EPA, RT-0400675, available at: http://www.camx.com/publ/pdfs/cb05_final_report_120805.pdf (last access: February 2014), 2005. 31049

Zhang, Q., Streets, D. G., Carmichael, G. R., He, K. B., Huo, H., Kannari, A., Klimont, Z., Park, I. S., Reddy, S., Fu, J. S., Chen, D., Duan, L., Lei, Y., Wang, L. T., and Yao, Z. L.: Asian emissions in 2006 for the NASA INTEX-B mission, Atmos. Chem. Phys., 9, 5131–5153, doi:10.5194/acp-9-5131-2009, 2009. 31050

ACPD
14, 31039–31090, 2014

Zhang, R., Bian, Q., Fung, J. C., and Lau, A. K.: Mathematical modeling of seasonal variations in visibility in Hong Kong and the Pearl River Delta region, Atmos. Environ., 77, 803–816, doi:10.1016/j.atmosenv.2013.05.048, 2013. 31065

Zhou, Y., Brunner, D., Boersma, K. F., Dirksen, R., and Wang, P.: An improved tropospheric NO_2 retrieval for OMI observations in the vicinity of mountainous terrain, Atmos. Meas. Tech., 2, 401–416, doi:10.5194/amt-2-401-2009, 2009. 31042

Zhou, Y., Brunner, D., Spurr, R. J. D., Boersma, K. F., Sneep, M., Popp, C., and Buchmann, B.: Accounting for surface reflectance anisotropy in satellite retrievals of tropospheric NO_2, Atmos. Meas. Tech., 3, 1185–1203, doi:10.5194/amt-3-1185-2010, 2010. 31042, 31052, 31056

Zyrichidou, I., Koukouli, M. E., Balis, D. S., Kioutsioukis, I., Poupkou, A., Katragkou, E., Melas, D., Boersma, K., and van Roozendael, M.: Evaluation of high resolution simulated and OMI retrieved tropospheric NO_2 column densities over Southeastern Europe, Atmos. Res., 122, 55–66, doi:10.1016/j.atmosres.2012.10.028, 2013. 31043

ACPD
14, 31039–31090, 2014

Table 1. Ancillary parameters used for deriving tropospheric NO_2 column densities from OMI.

	Standard Product (SP2)	HK Retrieval (this work)
surface reflectance	OMI LER (5 year, monthly climatology, 0.5° × 0.5°)	MODIS MCD43C2 black-sky albedo (every 8 days, 0.05° × 0.05°)
surface pressure	GMI (2° × 2.5°, adjusted for elevation)	WRF (3 km × 3 km)
cloud pressure and fraction	OMI O_2–O_2 cloud algorithm	OMI O_2–O_2 cloud algorithm
aerosol optics	implicit	CMAQ (3 km × 3 km)
NO_2 profile shapes	GMI (multi-year monthly climatology, 2° × 2.5°)	CMAQ (3 km × 3 km)
temperature profiles	GEOS-5 (monthly)	WRF (3 km × 3 km)
RTM	TOMRAD	SCIATRAN
AMF calculation	interpolated from a look-up table	pixel-specific (no look-up table)
pixel sensitivity	centre point	instrument function

ACPD
14, 31039–31090, 2014

Table 2. Standard set of ancillary parameters used in the AMF sensitivity study.

Ancillary Parameter	Value
solar zenith angle (SZA)	48°
viewing zenith angle (VZA)	0° (nadir)
relative azimuth angle (RAA)	180°
terrain height	0.0 km
surface reflectance	0.05
aerosol/cloud radiance fraction	0.00
temperature and pressure profiles	WRF average
NO_2 and aerosol profiles	CMAQ averages (see Fig. 2)

ACPD
14, 31039–31090, 2014

Table 3. The AMFs for different aerosol treatment cases for the standard parameters and profiles (Fig. 2).

	PRD-1	PRD-2		PRD-3 & 4	
		clean	polluted	clean	polluted
NO_2 clean	0.84	0.68	0.39	0.77	0.74
NO_2 polluted	0.82	0.65	0.35	0.74	0.70

ACPD
14, 31039–31090, 2014

Table 4. The difference between raw and processed CMAQ data due to the spatial resolution of the satellite instrument (area averaging error).

	IOA	r	MB[a]	NMB[b]	RMSE[a]	CV[b]
HK & SZ	0.54	+0.25	−4.6	−16	17.6	59
FS & GZ	0.77	+0.67	−1.6	−12	7.0	52
all stations	0.69	+0.56	−2.9	−17	9.3	54

[a] in ppbv, [b] in percent.

ACPD
14, 31039–31090, 2014

Table 5. OMI evaluation with the RAQM network.

Case	IOA	r	MB[a]	NMB[b]	RMSE[a]	CV[b]
Hong Kong and Shenzhen						
SP2	0.31	+0.19	−17.5	−54	23.4	73
PRD-1	0.43	+0.24	−8.8	−27	20.6	64
PRD-2	0.52	+0.25	−0.7	−2	21.9	68
PRD-3	0.44	+0.20	−6.3	−20	20.7	64
PRD-4	0.45	+0.24	−7.4	−23	20.1	62
Foshan and Guangzhou						
SP2	0.43	+0.47	−14.3	−48	20.9	71
PRD-1	0.48	+0.41	−10.7	−36	19.2	65
PRD-2	0.58	+0.42	−5.2	−18	17.8	60
PRD-3	0.50	+0.40	−8.5	−29	18.4	62
PRD-4	0.53	+0.46	−8.7	−29	17.9	60
All stations						
SP2	0.40	+0.35	−10.7	−41	18.7	73
PRD-1	0.46	+0.31	−5.6	−22	18.2	71
PRD-2	0.53	+0.32	+0.7	+3	19.6	76
PRD-3	0.47	+0.29	−3.3	−13	18.6	72
PRD-4	0.50	+0.35	−3.9	−15	17.6	68

[a] in ppbv, [b] in percent.

ACPD
14, 31039–31090, 2014

Table 6. NO_2 mean values (in ppbv) at the RAQM network stations for CMAQ, network and OMI datasets.

Stations	CMAQ (raw)	CMAQ (processed)	RAQM	SP2	PRD-1	PRD-2	PRD-3	PRD-4
HK & SZ	29.3	25.1	32.9	14.9	23.4	31.6	25.9	24.8
FS & GZ	13.7	12.0	29.5	15.2	18.9	24.4	21.0	20.8
All stations	18.6	15.7	25.3	14.5	19.4	25.6	21.6	21.0

ACPD
14, 31039–31090, 2014

Table 7. Evaluation of the time series of CMAQ with OMI NO_2 VCDs in the two areas marked in Fig. 4.

Dataset	OMI Mean[a]	IOA	*r*	MB[a]	NMB[b]
Foshan and Guangzhou (area)					
SP2	2.5	0.57	0.37	−0.5	−18
PRD-1	3.1	0.55	0.35	−1.1	−35
PRD-2	4.0	0.51	0.35	−2.0	−49
PRD-3	3.5	0.56	0.43	−1.5	−42
PRD-4	3.4	0.54	0.37	−1.3	−40
Hong Kong and Shenzhen (area)					
SP2	1.7	0.51	0.57	+1.2	+73
PRD-1	2.4	0.65	0.51	+0.6	+24
PRD-2	3.2	0.66	0.45	−0.2	−8
PRD-3	2.7	0.75	0.58	+0.2	+9
PRD-4	2.6	0.71	0.56	+0.4	+15

[a] in 10^{16} molecules cm^{-2}, [b] in percent.

ACPD
14, 31039–31090, 2014

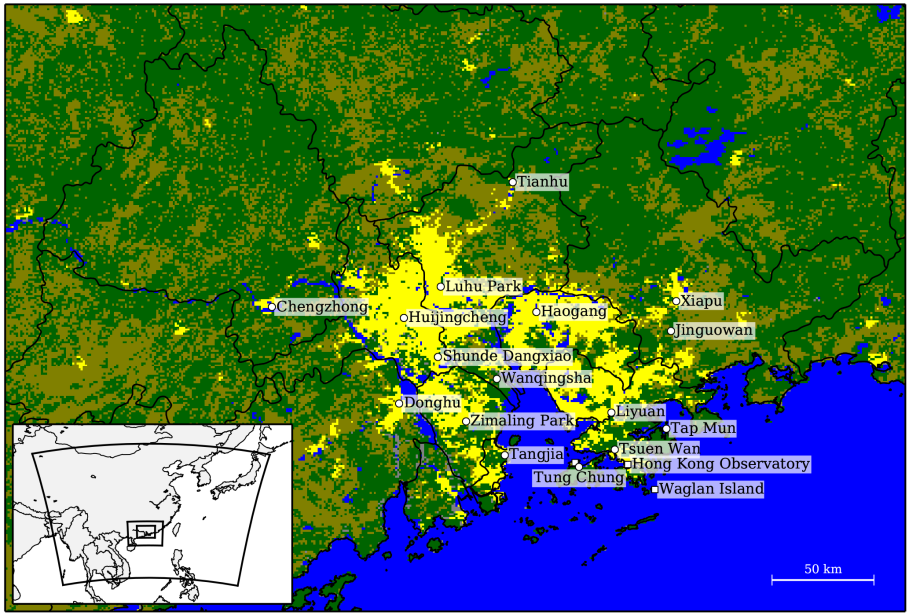

Figure 1. The large figure shows the CMAQ model domain (D3) with MODIS land categories in the Pearl River Delta (PRD) region grouped into the following categories: forest (darkgreen), crop lands (olive), bare land (grey), urban areas (yellow) and water (blue). The stations of the PRD Regional Air Quality Monitoring (RAQM) network and HKO automatic weather stations are marked by circles and squares, respectively. The small figure shows the three CMAQ model domains which are D1, D2 and D3 from the largest to smallest.

ACPD
14, 31039–31090, 2014

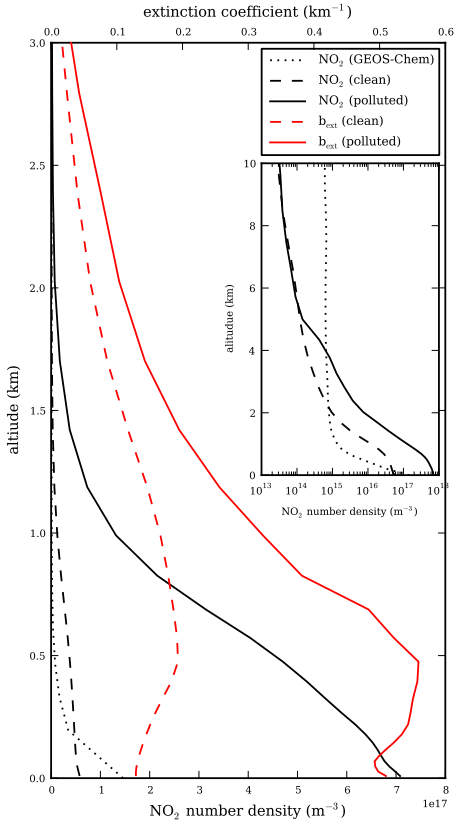

Figure 2. Averaged CMAQ NO_2 and b_{ext} profiles under "clean" and "polluted" conditions. A NO_2 profiles was categorised as polluted, if the ground number density was larger than 4.8×10^{17} m^{-3} (about 20 ppbv). A b_{ext} profile was categorised as polluted, if the ground extinction coefficient was larger than 0.4. The clean b_{ext} profile has an AOT of 0.3 while the polluted as an AOT of 0.6. In addition, an annual GEOS-Chem NO_2 profile is shown for Hong Kong ($2^\circ \times 2.5^\circ$ spatial resolution).

ACPD
14, 31039–31090, 2014

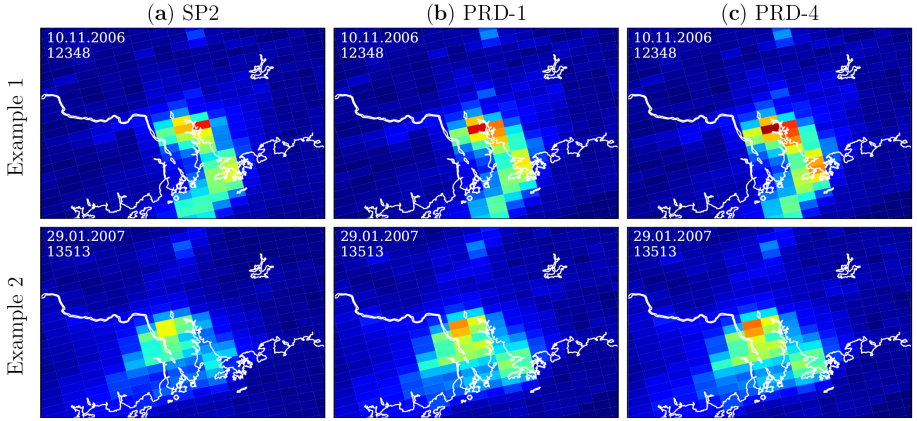

Figure 3. Two example orbits of OMI NO_2 distributions for SP2, PRD-1 and PRD-4. The overall spatial distribution is similar but different in details. The PRD-1 and PRD-4 datasets have larger NO_2 column densities than the standard product (SP2).

ACPD
14, 31039–31090, 2014

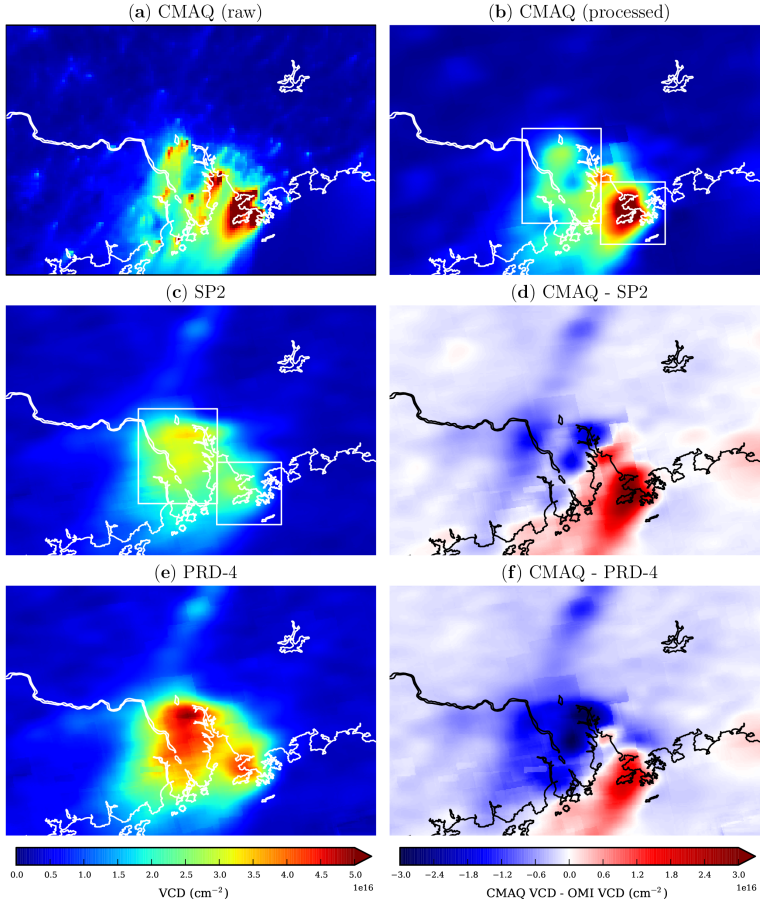

Figure 4. Four-month mean distribution of **(a)** raw and **(b)** processed CMAQ NO_2 VCDs, **(c)** OMI SP2 VCDs and **(d)** the difference to CMAQ, **(e)** OMI PRD-4 VCDs and **(f)** the difference to CMAQ.

ACPD
14, 31039–31090, 2014

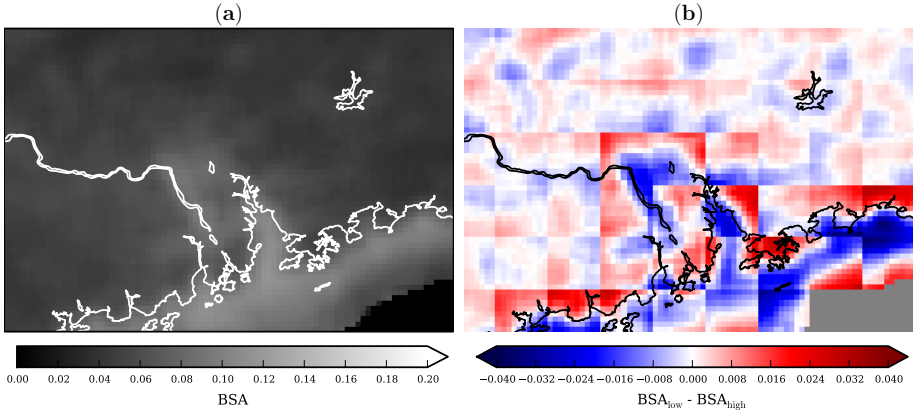

Figure 5. (a) The averaged MODIS black-sky albedo (BSA) and **(b)** the differences between low- and high-resolution BSAs.

ACPD
14, 31039–31090, 2014

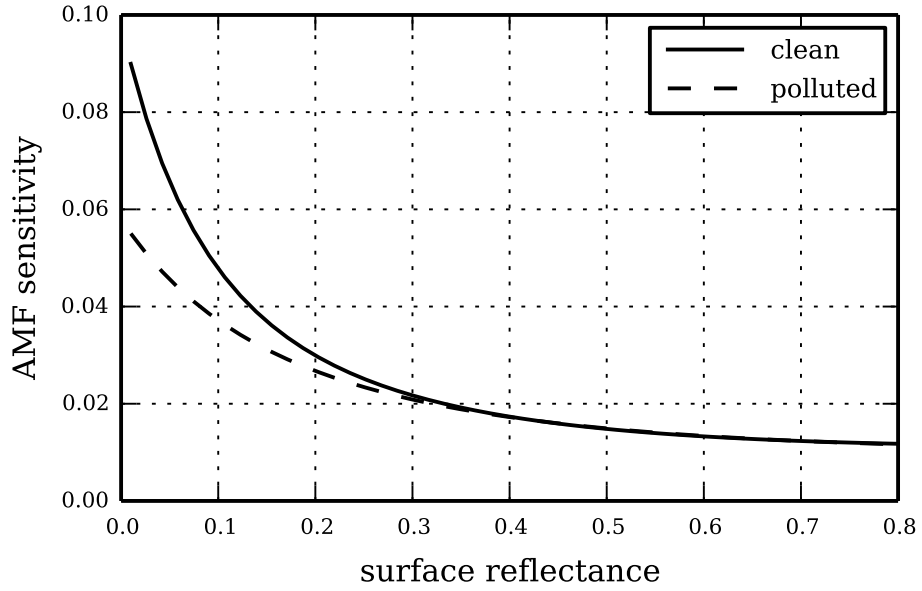

Figure 6. Sensitivity of AMF to a change of 0.01 in surface reflectance for different surface reflectance. The lines show the sensitivity for a polluted and clean aerosol profile (Fig. 2).

ACPD
14, 31039–31090, 2014

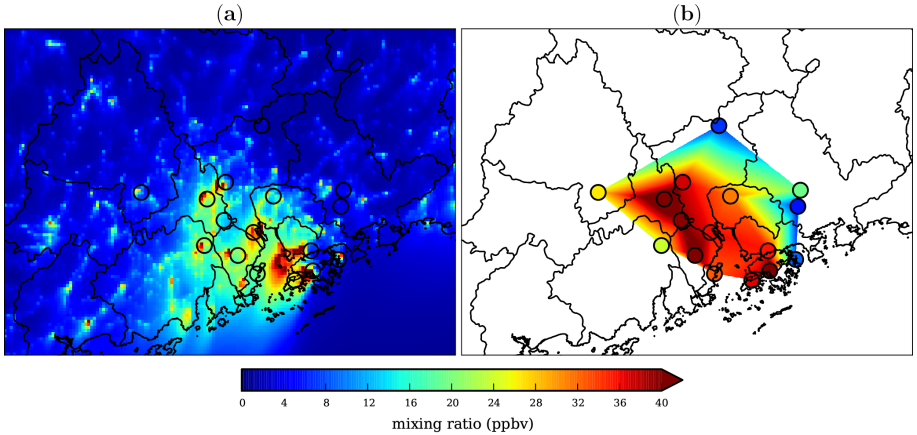

Figure 7. Ground level NO_2 mixing ratios averaged for October 2006 to January 2007: **(a)** CMAQ simulation and **(b)** RAQM network measurements. The values between stations have been estimated by linear interpolation.

ACPD
14, 31039–31090, 2014

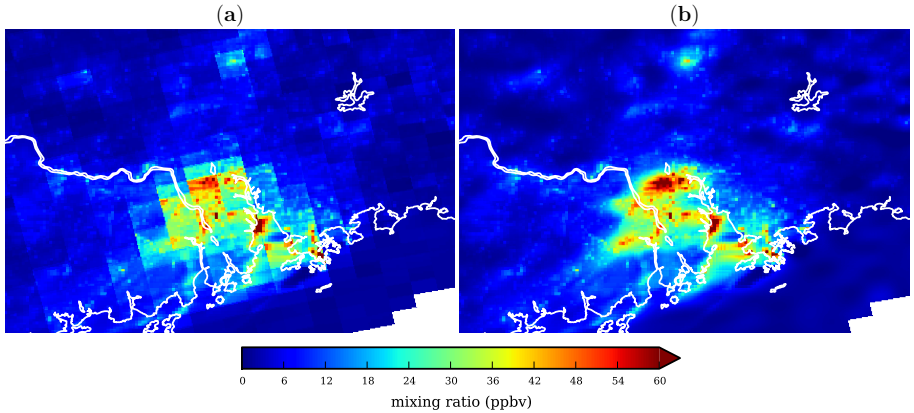

Figure 8. OMI ground mixing ratios from orbit number 13513 on 29 January 2007 comparing a **(a)** "standard" and **(b)** newly developed gridding algorithm (Kuhlmann et al., 2014). The discontinuous map created by the "standard" algorithm is difficult to interpret while the new algorithms makes an analysis of the spatial distribution easier.

ACPD
14, 31039–31090, 2014

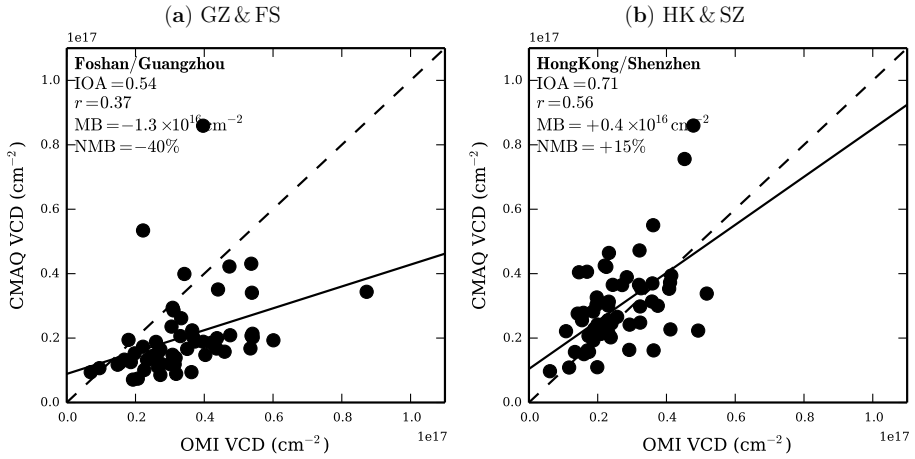

Figure 9. Scatter plot between CMAQ and PRD-4 at **(a)** GZ & FS and **(b)** HK & SZ.

ACPD
14, 31039–31090, 2014